





Delayed fragmentation of ethylene and allene induced by electron impactLong Wei ^{1,2}, Baihui Ren,^{1,2} Yu Zhang ^{3,*}, Jiarong Wang ^{1,2}, Bo Wang,^{1,2} Jie Han,^{1,2} Wandong Yu,^{1,2} Yaming Zou,^{1,2} Li Chen,^{1,2} and Baoren Wei ^{1,2,†}¹*Institute of Modern Physics, Fudan University, Shanghai 200433, China*²*Key Laboratory of Nuclear Physics and Ion-Beam Application (MOE), Fudan University, Shanghai 200433, China*³*School of Mathematics, Physics and Information Engineering, Jiaxing University, Jiaxing 314001, China*

(Received 30 September 2020; accepted 5 January 2021; published 19 January 2021)

We experimentally investigated the delayed fragmentation processes of ethylene and allene dications induced by 300-eV electrons with the cold target recoil ion momentum spectroscopy in an observation window up to $\sim 2 \mu\text{s}$. For each molecule, several distinct pathways involving prompt or delayed fragmentations were observed and relative branching ratios among them were analyzed. According to the time-of-flight coincidence measurements of corresponding recoil ionic fragments, the survival times and thus lifetimes from nanoseconds to microseconds of different delayed-dissociative precursor dications were retrieved. Besides the two-body channels, i.e., $\text{H}^+ + \text{C}_2\text{H}_3^+$ and $\text{H}^+ + \text{C}_3\text{H}_3^+$, the delayed deprotonation was also observed in many-body channels, i.e., $\text{H} + \text{H}^+ + \text{C}_n\text{H}_2^+$ ($n = 2, 3$) and $2\text{H}/\text{H}_2 + \text{H}^+ + \text{C}_3\text{H}^+$. The lifetimes of the metastable intermediate diacations $\text{C}_n\text{H}_3^{2+}$ and $\text{C}_3\text{H}_2^{2+}$ were estimated.

DOI: [10.1103/PhysRevA.103.012810](https://doi.org/10.1103/PhysRevA.103.012810)**I. INTRODUCTION**

In the past decades, the ionization and fragmentation of molecules, especially of astrophysical or biological significance, induced by various excitation methods, e.g., electron impact, photoionization, and highly charged ion (HCI) collision, have attracted much attention [1–6]. A hot topic in this area is the evolution dynamics of the ionized molecules in different sizes, ranging from simple molecules or small clusters to biological macromolecules [7–15]. Those multi-charged molecular ions, if unstable, could undergo prompt or delayed dissociation and thus lead to the formation of fragments that have unique nature or important functions [5,15]. The lifetime of an unstable molecular ion plays a vital role in understanding molecular properties and chemical reactions [7,9,16]. For the prompt or direct dissociation process, the time scale is usually short, e.g., in the order of femtosecond for fast Coulomb explosion of dicationic or multiply charged molecules [17]. The time, on the other hand, can be several tens to hundreds of femtoseconds, if the molecular ions proceed with sequential dissociation [7] or significant structural rearrangements, e.g., proton or hydrogen migration and isomerization [4,8,16,18,19], before the formation of resultants. An example for such kind of process is the long lifetime H_2 roaming process [16,18,20], which could last up to ~ 500 fs and has been recently revealed as a dominant pathway to form H_3^+ from organic molecular dications [20].

However, in the delayed fragmentation process, the time scale of molecular dissociation can be extended from nanoseconds to microseconds, due to the quite long lifetime of the

metastable molecular ion prior to dissociation. In recent years, such delayed processes have been observed for two-body fragmentation of various molecular dications [10,11,14,21–32]. Employing the three-dimensional momentum imaging technique, the survival times of different metastable dications have been retrieved and analyzed by a single- [14,23–26] or two-term [22,27] exponential fitting to obtain the dication lifetimes. The divergence of lifetimes was observed for isotope molecules ($\text{C}_2\text{H}_4^{2+}$ and $\text{C}_2\text{D}_4^{2+}$) [22], but not for isomer molecules (propyne and allene) [31]. Besides the exponential decay, the power-law decay which is a statistical law of decay, has been used to explain the two-body deprotonation fragmentation of $\text{C}_2\text{H}_4^{2+}$ and $\text{C}_3\text{H}_4^{2+}$ [27,31]. In addition to the lifetime information, the kinetic energy release (KER) of the delayed fragmentation can be obtained. The KERs of CO_2^{2+} and $\text{C}_2\text{H}_4^{2+}$ delayed channels were found almost the same as those of corresponding prompt channels [22,23,26], but discrepancies were observed in the case of HCl^{2+} [24]. On the theoretical side, the delayed fragmentation process was interpreted by the quantum chemistry calculations as due to the tunneling of specific vibrational states on a dicationic electronic state [23].

Although much has been learned about two-body delayed dissociation, less is known about many-body processes. In this work, the delayed fragmentation of two alkene hydrocarbon molecules, i.e., ethylene and allene (CH_2CH_2 and CH_2CCH_2), colliding with 300-eV electrons, was studied with the cold target recoil ion momentum spectroscopy (COLTRIMS) technology. The observation windows for metastable decay of ethylene and allene dications were enlarged to ~ 2.3 and $\sim 2.7 \mu\text{s}$, respectively, which are conducive to the study of long-lived dissociation processes. The survival times of different metastable dications were retrieved by the coincidence measurements of recoil ionic fragments. In addition

*zyclay@outlook.com

†brwei@fudan.edu.cn

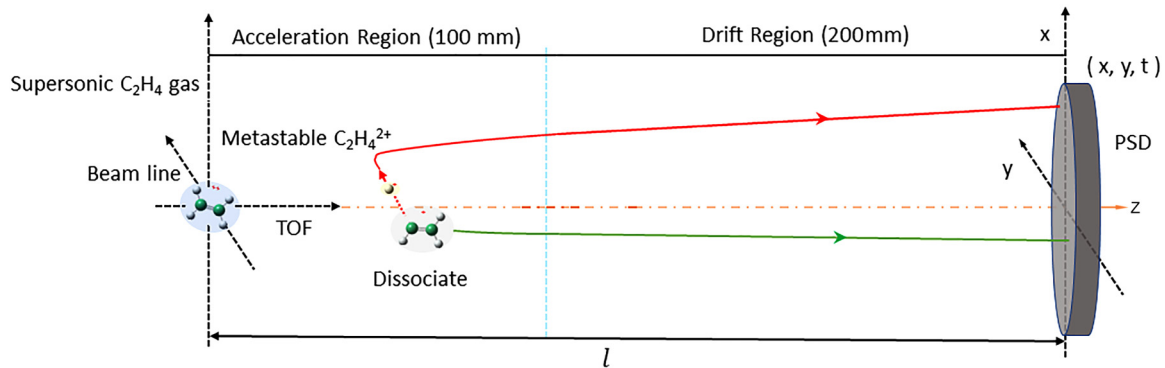


FIG. 1. Schematic of the fly traces of ionic fragments in the TOF windows. l represents the flight distance between collision center and PSD. The acceleration region and drift region are 100 and 200 mm long, respectively. y axis is defined by the electron beam, and x axis by the molecular beam, z corresponds to the TOF (t) axis.

to the lifetime of two-body delayed deprotonation channels $C_nH_4^{2+} \rightarrow H^+ + C_nH_3^+$ ($n = 2, 3$), we also analyzed the many-body channels $C_nH_4^{2+} \rightarrow H + H^+ + C_nH_2^+$ and $C_3H_4^{2+} \rightarrow 2H/H_2 + H^+ + C_3H^+$ and obtained the lifetimes of corresponding precursor dications.

II. EXPERIMENT METHOD

The experiments of fragmentation of ethylene and allene induced by 300-eV electron impact were carried out using the COLTRIMS technology at Fudan University. The experimental setup and principle have been described in detail in previous work [33]. In brief, an electron beam perpendicularly crossed a supersonic jet which was produced when molecules escaped from a high pressure (1 bar), high purity (99.99%) gas passing through a 10- μ m nozzle into the high vacuum interaction chamber. After a collision, the transmitted electron pulse was collected by a Faraday cup. The recoil ions were extracted and analyzed with a Wiley-McLaren time-of-flight (TOF) spectrometer which was equipped with a position-sensitive detector (PSD) composed of two microchannel plates and delay-line anode readout. To determine the TOF of each ion, the hitting times of the recoil ions on the PSD were recorded by a multihit time-digital converter (TDC) for which the pulsed signal of the electron gun served as the time reference. The time resolution of the TDC was 25 ps. As shown in Fig. 1, the two-dimensional momentum position information (x, y) and the TOF (t) of each recoil ion were recorded. From these (x, y, t) parameters, the three-dimensional momenta of the ion were determined. The extraction field in the TOF spectrometer was 60 V/cm; it ensured that recoil ions of kinetic energy (KE) smaller than 5.5 eV could be collected in a 4π solid angle for prompt decay. Meanwhile, with such a weak extraction field, delayed fragmentations (KE < 5.5 eV) occurring within the time scale of $< \sim 2 \mu$ s could be completely collected both for ethylene and allene dications. The species of a detected ion was identified by the relationship between the TOF and the mass-to-charge ratio. The fragmentation channels were identified by the ion-ion mass coincidence map. During the experiment, a pair of coils was used to counteract the influence of the geomagnetic field in the collision chamber, and the base pressure was better than 3×10^{-10} Torr. The apparatus and measurement were calibrated using the double ionization

of N_2 . The resolution of the TOF was about 10 ns, which was mainly limited by the property of the apparatus and the measurement system.

III. RESULTS AND DISCUSSION

A. Identification of delayed fragmentation and retrieving the survival time

Figure 2 shows typical coincidence TOF (CTOF) spectra of the fragmentation of ethylene and allene molecules induced by 300-eV electron impact. The TOF of the first detected recoil ion was plotted along the horizontal axis and that of the second ion along the vertical axis. Apart from coincidence islands of different ion pairs, long “tails” can be noticed in Figs. 2(a) and 2(b). They are attached to coincidence islands of several ion pairs, such as $H^+ + C_2H_3^+$ and $H^+ + C_2H_2^+$ in Fig. 2(a) and $H^+ + C_3H_3^+$, $H^+ + C_3H_2^+$, and $H^+ + C_3H^+$ in Fig. 2(b).

Such “tail” structures have been observed in many experiments [11,14,21–32] and attributed to delayed fragmentation of metastable molecular ions. A molecular ion in an excited state after collision ionization could undergo radiative de-excitation or dissociation. Prompt dissociations on a time scale of femtosecond or picosecond lead to the intense islands plotted around the nominal TOFs of the two involved fragments. Due to the initial velocities of the two partners obtained during the fast Coulomb repulsion process, their TOFs, TOF_1 and TOF_2 , are modified comparing to their respective nominal TOFs. According to the momentum conservation, the relation, $TOF_1 + TOF_2 = \text{constant}$, should be verified, leading to the typical inclined islands as shown in Fig. 2. However, if the dissociation occurs in the acceleration region of the TOF window with a delay time scale of a nanosecond or even longer, the TOF becomes longer for the light fragment and shorter for the heavy fragment with respect to their nominal TOFs. This leads to the appearance of the long “tails” observed in the coincidence map. A tail in the CTOF map runs from the nominal TOFs of the corresponding fragments to an asymptotic point characterized by $TOF_1 = TOF_2$ equal to the TOF of the corresponding doubly charged metastable precursor ion. Indeed, if the dissociation occurs in the field-free drift region of the TOF window, the two partners flying with the velocity of the precursor ion could not be differentiated. This provides indirect

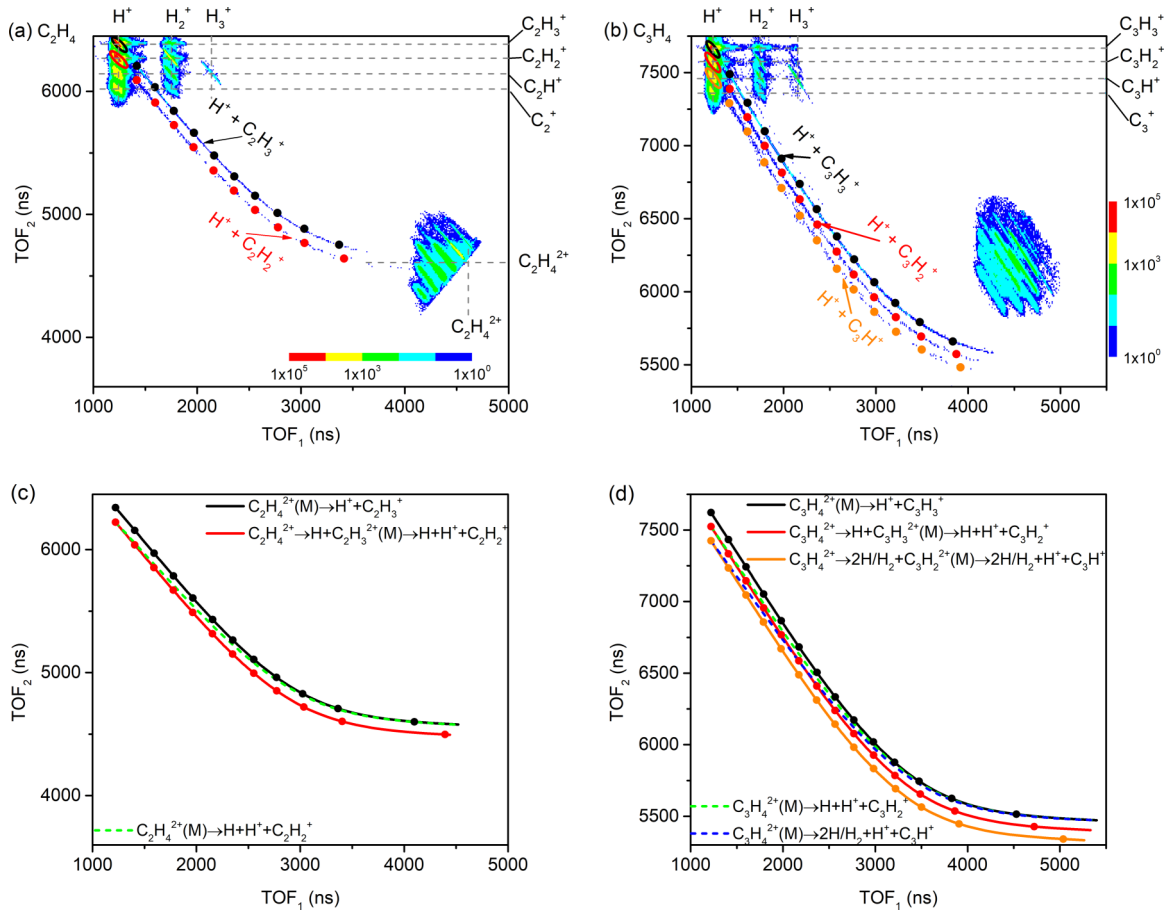


FIG. 2. The measured coincidence time-of-flight spectra with (a) C_2H_4 and (b) C_3H_4 , respectively. The black, red, and yellow dots represent events with $KER = 0$ and delay times of n 200 ns with $n = 1, 2, 3 \dots$ Panels (c) and (d) are the simulated coincidence time-of-flight spectra of various delayed fragmentation channel for C_2H_4 and C_3H_4 , respectively.

evidence for the existence of metastable precursor dications. In following, we will focus on the delayed fragmentations of metastable double-ionization dications $C_2H_4^{2+}$, $C_3H_4^{2+}$, and some secondary dications (metastable intermediate ions) $C_2H_3^{2+}$, $C_3H_3^{2+}$, and $C_3H_2^{2+}$.

To study the delayed dissociation of metastable molecule ions, we have determined the delay time or the survival time t_d of the precursor ions from the long tail structures. Combining the apparatus parameters (see Fig. 1) and the Newton's motion equations of fragment ions, the survival time t_d is involved in the following equations:

$$l_1 = \frac{1}{2}a_m t_d^2 + (a_m t_d + v_{jz})t_{j1} + \frac{1}{2}a_j t_{j1}^2, \quad (1)$$

$$l_2 = (a_m t_d + v_{jz} + a_j t_{j1})t_{j2}, \quad (2)$$

$$\sum_{j=1}^2 m_j v_{jz} = 0, \quad (3)$$

$$TOF_j = t_d + t_{j1} + t_{j2}, \quad (4)$$

where the index $j = 1, 2$ represents the two dissociation products. l is the distance from the center of the collision to the PSD, $l = l_1 + l_2$, l_1 and l_2 are the lengths of acceleration and drift regions, respectively. $a_m = qE/m$ is the acceleration

of the precursor dications in the extraction region, q and m are the charge and mass of the dication, respectively. E is the uniform electric field strength of the extraction region. a_j is the acceleration of different fragments in the extraction region. t_d is the survival time corresponding to the fly time between the collision center and the moment when the fragmentation occurs, t_{j1} and t_{j2} are the flight time of the fragment j in extraction and drift regions respectively. In addition, before the ions fly out of the drift region and hit on the MCP detector, they need to pass through a 10-mm-long region with electric field of ~ 1400 V/cm. The flight time in this higher field is only tens of nanoseconds to 100 nanoseconds, which is much less than the TOFs ($< 2\%$) of recoil ions, and thus has little influence on the calculation of t_d and lifetime. Here v_{jz} stands for the z component velocity of the fragments along the TOF axis, resulting from the energy release accompanying the fragmentation. The mean value of v_{jz} is zero and v_{jz} is reasonably small compared with the additional velocity gained in the extraction field [22], so in the following, these terms will be ignored for simplification. The absolute detection efficiency of MCP for protons and heavy recoil fragments released at different dissociation decay times is considered to be constant. Finally, for each couple of measured TOF_j , the corresponding survival time t_d of the molecular dication was obtained by solving Eqs. (1)–(4). Then

the measured fragment number distribution as a function of the TOF_{*j*} was converted to a count distribution as a function of t_d . It is worth mentioning that when the dissociation decay occurs in the field-free drift region, the t_d could not be simply solved with this method. From the above calculations we found that the time scales for the ethylene and allene dications flying through the acceleration region and drift zone are ~ 2.3 and $\sim 2.7 \mu\text{s}$, respectively. These time values correspond to lifetime sensitive observation windows of our experiment for the studied molecules. Fortunately, all tails in Fig. 2 present a negligible count as approaching the associated asymptotic points, showing that our lifetime observation windows were large enough for studying the dissociation processes in this work.

B. Delayed decay scheme and lifetime information of metastable parent dications

If a population $N(t)$ of metastable dications decays with a lifetime τ , it is described simply by the exponential function,

$$N(t) = N_0 e^{-t/\tau}, \quad (5)$$

where N_0 refers to the count of the precursor metastable molecular dications prepared in the interaction with electrons. The dissociation count number ΔN measured in a time

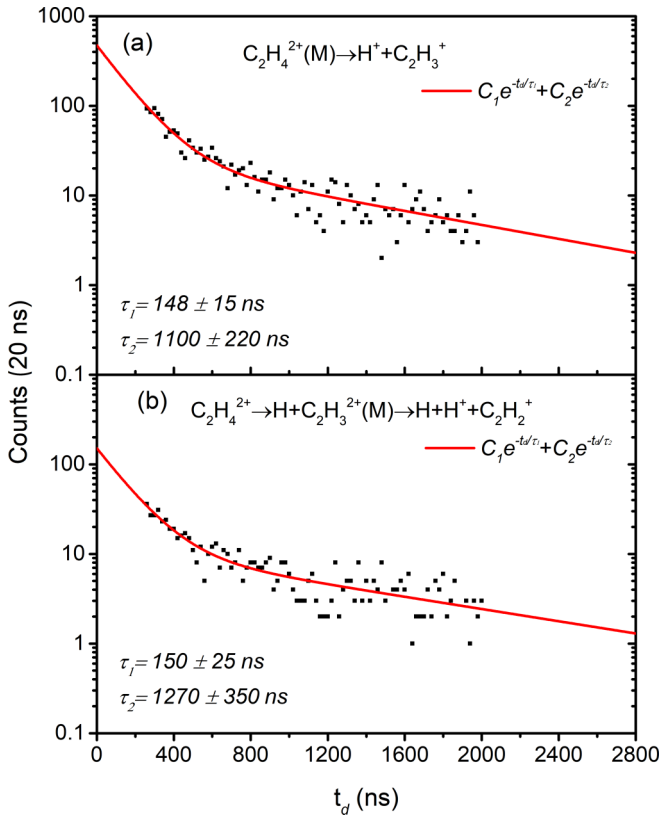


FIG. 3. Semilogarithmic histogram of the survival time of delayed dissociation decay of metastable dication for ethylene induced by 300-eV electrons. Corresponding exponential fits are shown by red solid lines. “(M)” is the abbreviation for “metastable,” which represents the metastable parent ion corresponding to the delayed dissociation.

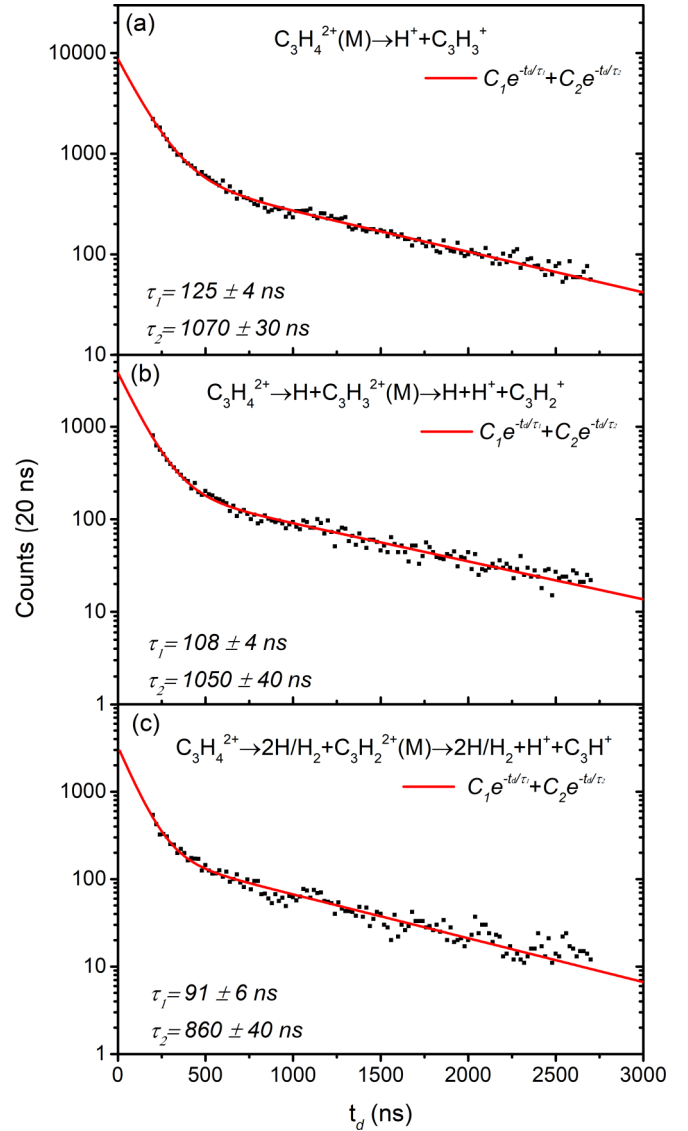


FIG. 4. Semilogarithmic histogram of the survival time of delayed dissociation decay of metastable dication for allene induced by 300-eV electrons. Corresponding exponential fits are shown by red solid lines.

interval Δt around the dissociation time t_d is then proportional to the law of exponential decay, as follows:

$$\Delta N(t_d) = N_0 \frac{1}{\tau} e^{-t_d/\tau} \Delta t = C e^{-t_d/\tau} \Delta t, \quad (6)$$

where C is a constant. In Figs. 3 and 4, we plotted the fragment yields in time intervals of 20 ns as a function of the converted dissociation time t_d for ethylene and allene molecules, respectively. Events occurring within shorter dissociation time, $t_d < 200$ ns, were contributed by both the prompt and delayed dissociation which could not be effectively separated due to the time broadening caused by KEs of the fragments [Figs. 2(a) and 2(b)]. Therefore, data in such a short time range are not considered here, only data points in a longer dissociation time range are presented in Figs. 3 and 4. In these figures, one can notice that all fragment yields plotted in a semilogarithmic scale present a similar decay behavior with two distinct slopes.

TABLE I. The lifetimes of the delayed fragmentation channels of $\text{CH}_2\text{CH}_2^{2+}$ and $\text{CH}_2\text{CCH}_2^{2+}$, extracted by two-term exponential fit.

	Delayed channel									
	$\text{CH}_2\text{CH}_2^{2+}$ (ethylene)				$\text{CH}_2\text{CCH}_2^{2+}$ (allene)					
	$\text{H}^+ + \text{C}_2\text{H}_3^+$		$\text{H} + \text{H}^+ + \text{C}_2\text{H}_2^+$		$\text{H}^+ + \text{C}_3\text{H}_3^+$		$\text{H} + \text{H}^+ + \text{C}_3\text{H}_2^+$		$2\text{H}/\text{H}_2 + \text{H}^+ + \text{C}_3\text{H}^+$	
Lifetime (ns)	τ_1	τ_2	τ_1	τ_2	τ_1	τ_2	τ_1	τ_2	τ_1	τ_2
Present work	148 ± 15	1100 ± 220	150 ± 25	1270 ± 350	125 ± 4	1070 ± 30	108 ± 4	1050 ± 40	91 ± 6	860 ± 40
Jochim <i>et al.</i> ^a	202 ± 10	916 ± 40								
Larimian <i>et al.</i> ^b		498 ± 12								
Takahashi <i>et al.</i> ^c	<40	$60\text{--}800$								
Yuan <i>et al.</i> ^d					93 ± 7					

^aReference [22].

^bReference [23].

^cReference [27].

^dReference [31].

This is characteristic of contributions from two populations with two dissociation lifetimes. In the following, the fragment yield decays will be fitted using a two-term exponential decay function, $C_1 e^{-t/\tau_1} + C_2 e^{-t/\tau_2}$ to extract the lifetimes (τ_1 , τ_2) of the metastable precursor molecules.

In the case of the deprotonation channel of ethylene, $\text{C}_2\text{H}_4^{2+} \rightarrow \text{H}^+ + \text{C}_2\text{H}_3^+$, the fragment yield decay is presented in Fig. 3(a). It was retrieved from the tail attached to the ion pair $\text{H}^+ + \text{C}_2\text{H}_3^+$ in the CTOF spectrum in Fig. 2(a) (black dot). This tail starts from the $\text{H}^+ + \text{C}_2\text{H}_3^+$ island and ends at the TOF of the ‘‘ion pair’’ $\text{CH}_2^+ \text{--} \text{CH}_2^+$ corresponding in fact to the TOF of the parent ion $\text{C}_2\text{H}_4^{2+}$. The lifetimes of the metastable parent ions $\text{C}_2\text{H}_4^{2+}$ were extracted by two-term exponential function fitting, as shown in Fig. 3(a). The lifetimes of delayed deprotonation processes were found to be $\tau_1 = 148 \pm 15$ ns and $\tau_2 = 1100 \pm 220$ ns and displayed in Table I. These extracted lifetimes indicate that at least two different metastable states were involved in the delayed fragmentation process. The standard deviation of fitting was considered as errors. For this fragmentation channel, similar decay features with two lifetimes were observed in a previous experiment using intense laser pulses with 23 fs duration by Jochim *et al.* [22]. The reported lifetimes were found to be $\tau_1 = 202 \pm 10$ ns and $\tau_2 = 916 \pm 40$ ns, where τ_2 is in agreement with the present measurement in the limit of error, but a discrepancy appears in τ_1 . In experiments using strong femtosecond laser field with a pulse duration down to 4.5 fs, a single lifetime decay with $\tau = 498 \pm 12$ ns was observed by Larimian *et al.* [23]. In addition, this delayed channel was also observed in low- and medium-energy collisions of HCIs; a two-term exponential feature was reported with the faster component $\tau_1 < 40$ ns and the slower component $\tau_2 \sim 60\text{--}800$ ns [27]. In essence, the lifetime of metastable dications decay is closely related to the vibrational state and sensitive to the potential energy curve (PEC) and the structure of molecule species. Based on the calculation of one-dimensional PECs and the lifetimes for vibrational levels along one of the C-H distances of the ethylene dication with the planar geometry in Ref. [23], a dissociation lifetime of 1.3 μs was expected for high-lying ($v = 10$) vibrational states of the second excited (singlet) state $^1A'$ of $\text{C}_2\text{H}_4^{2+}$. The agreement of this value with our slow component lifetime τ_2

suggests that such states were possibly populated in collisions with a 300-eV electron beam. The discrepancy on the measured delayed dissociation lifetimes in different experiments reflects the population of different metastable states in interactions with laser pulse, highly charged ion, and electron, etc. Indeed, the ionization scheme and the excited states of the molecular ions strongly depend on the interaction conditions, such as the pulse duration of laser [34], collision energy and charge state of HCIs, and the incident energy of electrons. In the present work, taking advantage of the larger time observation window compared with those in the references, we were able to available study the delay decay with a longer lifetime.

In Fig. 2 near the delayed deprotonation channel of $\text{C}_2\text{H}_4^{2+}$, another tail attached to the ion pair $\text{H}^+ + \text{C}_2\text{H}_2^+$ can be also observed. Such an ion pair is produced from typical three-body fragmentation of ethylene dication. The undetected neutral H moiety could be released by prompt or delayed dissociation of $\text{C}_2\text{H}_4^{2+}$; the corresponding fragmentation pathway is the direct fragmentation, $\text{C}_2\text{H}_4^{2+}(\text{metastable}) \rightarrow \text{H} + \text{H}^+ + \text{C}_2\text{H}_2^+$, of the long-lived metastable dication $\text{C}_2\text{H}_4^{2+}$ or dissociation of an intermediate metastable dication $\text{C}_2\text{H}_3^{2+}$, i.e., $\text{C}_2\text{H}_4^{2+} \rightarrow \text{H} + \text{C}_2\text{H}_3^{2+}(\text{metastable}) \rightarrow \text{H} + \text{H}^+ + \text{C}_2\text{H}_2^+$. To clearly identify the reaction pathway, a simulation of time-of-flight mass spectrum which shows the different dissociation mechanism of precursor ions has been made in Fig. 2(c). Here, we assume $\text{KER} = 0$ eV of each fragmentation to simplify the calculation. As shown in Fig. 2(c), the green dashed line intersecting with other lines represents the delayed fragmentation pathway $\text{C}_2\text{H}_4^{2+}(\text{metastable}) \rightarrow \text{H} + \text{H}^+ + \text{C}_2\text{H}_2^+$, which is a delayed process of neutral H loss. In contrast, the red tail displays a two-step pathway: First, a C-H bond is promptly broken leading to an intermediate metastable $\text{C}_2\text{H}_3^{2+}$ dication and a neutral H moiety, i.e., $\text{C}_2\text{H}_4^{2+} \rightarrow \text{H} + \text{C}_2\text{H}_3^{2+}(\text{metastable})$, and then the metastable $\text{C}_2\text{H}_3^{2+}$ ion flies in the acceleration field and decays by delayed deprotonation, $\text{C}_2\text{H}_3^{2+}(\text{metastable}) \rightarrow \text{H}^+ + \text{C}_2\text{H}_2^+$. Furthermore, the black tail, which is simulated for the delayed two-body fragmentation $\text{C}_2\text{H}_4^{2+}(\text{metastable}) \rightarrow \text{H}^+ + \text{C}_2\text{H}_3^+$ of precursor $\text{C}_2\text{H}_4^{2+}$ dication, is in good agreement with the experimental result.

According to the above analysis, a conclusion can be drawn that the observed experimental tail of ion pair $\text{H}^+ + \text{C}_2\text{H}_2^+$ is

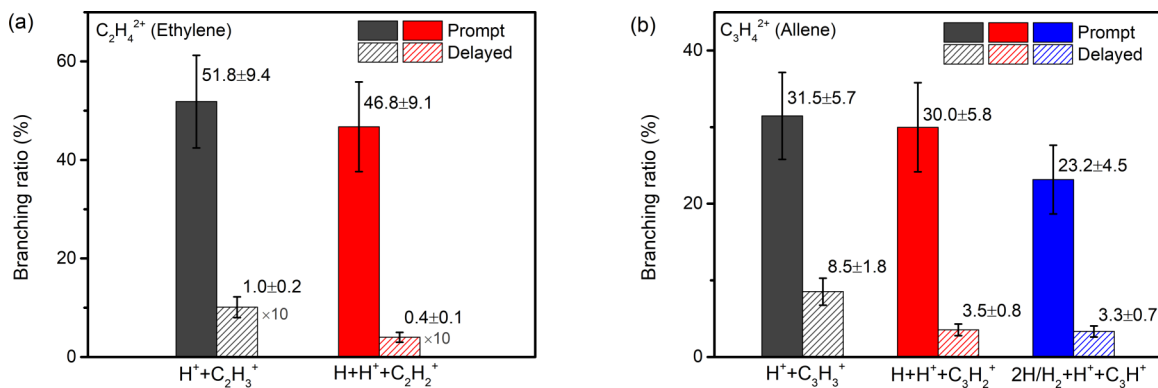


FIG. 5. Histogram diagram of branching ratios for prompt and delayed fragmentation channels of ethylene and allene dications, respectively.

assigned to the two-step dissociation process $C_2H_4^{2+} \rightarrow H + C_2H_3^{2+}$ (metastable) $\rightarrow H + H^+ + C_2H_2^+$. The associated fragment yield decay was obtained and shown in Fig. 3(b). The corresponding lifetimes of the metastable $C_2H_3^{2+}$ dications were extracted to be $\tau_1 = 150 \pm 25$ ns and $\tau_2 = 1270 \pm 350$ ns using the similar two-term exponential fit. However, in the earlier laser ionization dissociation experiments [22,23], the delayed dissociation of $C_2H_3^{2+}$ was not observed due to different ionization mechanisms. The double ionization in the strong field is most likely a sequential ionization process from the valence electrons [18,35], while for the present electron-impact ionization, two electrons are knocked out simultaneously and more internal energy could be deposited in the dication leading to the possibility to emit promptly a neutral H followed by the loss of a H^+ .

For the allene, another alkene molecule, the fragment yield decay for the involved delayed dissociation channels was obtained from the tails attached to the ion pairs $H^+ + C_3H_3^+$, $H^+ + C_3H_2^+$, and $H^+ + C_3H^+$ [see Fig. 2(b)] and is presented in Figs. 4(a)–4(c). As shown in Fig. 2(d), the many-body delayed fragmentation process also comes from the two-step pathway. The lifetimes of the corresponding precursor molecular dications, i.e., $C_3H_4^{2+}$, $C_3H_3^{2+}$, and $C_3H_2^{2+}$, were extracted and summarized in Table I. For the delayed two-body deprotonation fragmentation, the lifetimes of $C_3H_4^{2+} \rightarrow H^+ + C_3H_3^+$ were found to be $\tau_1 = 125 \pm 4$ ns and $\tau_2 = 1070 \pm 30$ ns. The faster component $\tau = 93 \pm 7$ ns was obtained from the collision with HCl's [31]. Unfortunately, due to the short TOF window in this previous work, decays with longer lifetime could not be observed, and our large observation window provides the possibility of observing long-lived metastable decay more effectively.

The deprotonation lifetimes of the other intermediate precursor ions were also estimated. For $C_3H_3^{2+} \rightarrow H^+ + C_3H_2^+$, we found $\tau_1 = 108 \pm 4$ ns and $\tau_2 = 1050 \pm 40$ ns. The metastable dication $C_3H_3^{2+}$ was produced by the prompt loss of a neutral H in the first step. For $C_3H_2^{2+} \rightarrow H^+ + C_3H^+$, the lifetimes are slightly shorter, $\tau_1 = 91 \pm 6$ ns and $\tau_2 = 860 \pm 40$ ns. The metastable dication $C_3H_2^{2+}$ was produced by $C_3H_4^{2+} \rightarrow 2H/H_2 + C_3H_2^{2+}$ (metastable) $\rightarrow 2H/H_2 + H^+ + C_3H^+$ which the neutral moiety ($2H/H_2$) was lost first followed by the delayed dissociation process. The measured lifetimes of $C_3H_n^{2+}$ ($n = 4, 3, 2$) show a

monotonous decreasing tendency with decreasing n or increasing number of lost H. It is noteworthy that delayed fragmentation involving the C = C bond stretching was not observed in the two studied alkene molecules. The rough reason could be that there is no tunneling potential barrier for C = C distance in such a nanosecond order, which has been supported by the PEC calculation of ethylene dication [9].

C. Relative branching ratios

The relative branching ratios of different dissociation channels involving prompt and delayed deprotonation from a parent dication were also analyzed. For a delayed channel, the initial population of the metastable dications was obtained by the summation of the contributions of the two components, $N_1 + N_2$, obtained from the adjusted parameters C_1 and C_2 [see Eq. (6)] found in the fitting procedure of the fragment yield decay curve [see Figs. 3 and 4]. For the prompt dissociation occurring in the order of femtosecond or picosecond, the production yield was estimated from the total count of the corresponding island on the CTOF map with subtracting the count due to the overlapped coincidence of metastable processes in the short time range. The obtained branching ratios are presented in Figs. 5(a) and 5(b) for ethylene and allene, respectively. The detection and collection efficiency were assumed to be consistent for arbitrary ion pairs, and the error bar was mainly contributed by the statistical errors. Moreover, the error caused by the limited experimental time resolution, which could be described by an error distribution function, was evaluated to be very small ($<3\%$), and was thus not considered here. The relative yield of a delayed metastable dissociation channel is systematically smaller than the corresponding prompt dissociation channel. The branching ratio of all delayed decay channels is about 1.4% for ethylene and about 15% for allene. Both the relative probabilities of prompt and delayed fragmentation channels show a decreasing trend with the loss of neutral hydrogen within the measurement error. Comparing Figs. 5(a) and 5(b), one can notice that the metastable dication formation probability increases with the growth of the carbon chain length. This tendency seems to suggest that for molecules with longer carbon chain, the larger vibrational degree of freedom and more complex electronic

configurations provide favorable conditions for the delayed deprotonation processes.

IV. CONCLUSIONS

In conclusion, we studied the delayed fragmentation in the microsecond time scale of ethylene and allene dications induced by 300-eV electron impact using the COLTRIMS. Several prompt and delayed channels from both dications were identified. From the CTOF spectra, we deduced the fragment yield decay curves of metastable precursor dications, which were fitted by a two-term exponential function. With a large TOF observation window $\sim 2 \mu\text{s}$, two lifetimes around 100 ns and 1 μs corresponding to two delayed deprotonation processes have been obtained for both metastable dications $\text{C}_2\text{H}_4^{2+}$ and $\text{C}_3\text{H}_4^{2+}$. Delayed deprotonation was also observed in the dissociation of secondary dications, i.e., $\text{C}_n\text{H}_3^{2+}$ ($n = 2, 3$) and $\text{C}_3\text{H}_2^{2+}$ after ultrafast loss of neutral hydro-

gen atom(s) from the parent dications. The lifetime of those secondary dications was analyzed, showing also two lifetimes which deviated slightly from those of parent dications $\text{C}_n\text{H}_4^{2+}$ ($n = 2, 3$). In particular for many-body channels of $\text{C}_3\text{H}_4^{2+}$, the lifetimes of $\text{C}_3\text{H}_4^{2+}$, $\text{C}_3\text{H}_3^{2+}$, and $\text{C}_3\text{H}_2^{2+}$ metastable dications decrease with the increasing number of lost neutral fragments. The relative branching ratios of different dissociation channels have been estimated. The quite significant relative branching ratios of delayed channels especially for allene dication indicate the important role of metastable state in molecular dissociation.

ACKNOWLEDGMENTS

This work was supported by the National Science Foundation of China under Contracts No. 11674067 and No. U1832201, and by the National Key Research and Development Program of China under Grant No. 2017YFA0402300.

- [1] F. Remacle and R. D. Levine, *Proc. Natl. Acad. Sci. USA* **103**, 6793 (2006).
- [2] D. Mathur, *Phys. Rep.* **225**, 193 (1993).
- [3] Z. Lu, Y. C. Chang, Q. Z. Yin, C. Y. Ng, and W. M. Jackson, *Science* **346**, 61 (2014).
- [4] S. Xu, D. Guo, X. Ma, X. Zhu, W. Feng, S. Yan, D. Zhao, Y. Gao, S. Zhang, X. Ren, Y. Zhao, Z. Xu, A. Dorn, L. S. Cederbaum, and N. V. Kryzhevoi, *Angew. Chem. Int. Ed.* **57**, 17023 (2018).
- [5] X.-D. Wang, X.-F. Gao, C.-J. Xuan, and S. X. Tian, *Nat. Chem.* **8**, 258 (2016).
- [6] Y. Zhang, L. Wei, C.-L. Yang, W. Yu, B. Wang, B. Yan, Y. Zou, L. Chen, and B. Wei, *Phys. Rev. A* **100**, 052706 (2019).
- [7] N. Neumann, D. Hant, L. Ph. H. Schmidt, J. Titze, T. Jahnke, A. Czasch, M. S. Schöffler, K. Kreidi, O. Jagutzki, H. Schmidt-Böcking, and R. Dörner, *Phys. Rev. Lett.* **104**, 103201 (2010).
- [8] A. Douhal, F. Lahmani, and A. H. Zewail, *Chem. Phys.* **207**, 477 (1996).
- [9] X. Xie, S. Roither, M. Schöffler, E. Lötstedt, D. Kartashov, L. Zhang, G. G. Paulus, A. Iwasaki, A. Baltuška, K. Yamanouchi, and M. Kitzler, *Phys. Rev. X* **4**, 021005 (2014).
- [10] L. H. Andersen, J. H. Posthumus, O. Vahtras, H. Ågren, N. Elander, A. Nunez, A. Scrinzi, M. Natiello, and M. Larsson, *Phys. Rev. Lett.* **71**, 1812 (1993).
- [11] P. Wang and C. R. Vidal, *Chem. Phys.* **280**, 309 (2002).
- [12] W. Iskandar, J. Matsumoto, A. Leredde, X. Fléchar, B. Gervais, S. Guillous, D. Hennecart, A. Méry, J. Rangama, C. L. Zhou, H. Shiromaru, and A. Cassimi, *Phys. Rev. Lett.* **114**, 033201 (2015).
- [13] X. Ren, E. Wang, A. D. Skitnevskaya, A. B. Trofimov, K. Gokhberg, and A. Dorn, *Nat. Phys.* **14**, 1062 (2018).
- [14] A. E. Slattery, T. A. Field, M. Ahmad, R. I. Hall, J. Lambourne, F. Penent, M. Ahmad, R. I. Hall, J. Lambourne, F. Penent, P. Lablanquie, and J. H. D. Eland, *J. Chem. Phys.* **122**, 084317(2005).
- [15] M. Eckstein, C.-H. Yang, M. Kubin, F. Frassetto, L. Poletto, H.-H. Ritze, M. J. J. Vrakking, and O. Kornilov, *J. Phys. Chem. Lett.* **6**, 419 (2015).
- [16] N. Ekanayake, T. Severt, M. Nairat, N. P. Weingartz, B. M. Farris, B. Kaderiya, P. Feizollah, B. Jochim, F. Ziaee, K. Borne, K. R. P. K. D. Carnes, D. Rolles, A. Rudenko, B. G. Levine, J. E. Jackson, I. Ben-Itzhak, and M. Dantus, *Nat. Commun.* **9**, 5186 (2018).
- [17] T. Yatsuhashi and N. Nakashima, *J. Photochem. Photobiol., C* **34**, 52 (2018).
- [18] E. Wang, X. Shan, L. Chen, T. Pfeifer, X. Chen, X. Ren, and A. Dorn, *J. Phys. Chem. A* **124**, 2785 (2020).
- [19] S. Maclot, D. G. Piekarski, A. Domaracka, A. Méry, V. Vizcaino, L. Adoui, F. Martín, M. Alcamí, B. A. Huber, P. Rousseau, and S. Díaz-Tendero, *J. Phys. Chem. Lett.* **4**, 3903 (2013).
- [20] Y. Zhang, B. H. Ren, C.-L. Yang, L. Wei, B. Wang, J. Han, W. Yu, Y. Y. Qi, Y. Zou, L. Chen, and B. Wei, *Commun. Chem.* **3**, 160 (2020).
- [21] T. A. Field and J. H. D. Eland, *Chem. Phys. Lett.* **211**, 436 (1993).
- [22] B. Jochim, R. Erdwien, Y. Malakar, T. Severt, B. Berry, P. Feizollah, J. Rajput, B. Kaderiya, W. L. Pearson, K. D. Carnes, A. Rudenko, and I. Ben-Itzhak, *New J. Phys.* **19**, 103006 (2017).
- [23] S. Larimian, S. Erattupuzha, E. Lötstedt, T. Szidarovszky, R. Maurer, S. Roither, M. Schöffler, D. Kartashov, A. Baltuška, K. Yamanouchi, M. Kitzler, and X. Xie, *Phys. Rev. A* **93**, 053405 (2016).
- [24] J. Ma, H. Li, K. Lin, Q. Song, Q. Ji, W. Zhang, H. Li, F. Sun, J. Qiang, P. Lu, X. Gong, H. Zeng, and J. Wu, *Phys. Rev. A* **97**, 063407 (2018).
- [25] A. Khan and D. Misra, *J. Phys. B: At. Mol. Opt. Phys.* **49**, 055201 (2016).
- [26] M. Alagia, P. Candori, S. Falcinelli, K.C. Mundim, M. S. P. Mundim, F. Pirani, R. Richter, S. Stranges, and F. Vecchiocattivi, *Chem. Phys.* **398**, 134 (2012).
- [27] K. Takahashi, K. Yokokawa, A. Mizumura, J. Matsumoto, H. Shiromaru, H. Kumar, P. Bhatt, and C. P. Safvan, *Phys. Rev. A* **98**, 062708 (2018).
- [28] D. A. Hagan and J. H. D. Eland, *Org. Mass Spectrom.* **27**, 855 (1992).

- [29] M. Alagia, C. Callegari, P. Candori, S. Falcinelli, F. Pirani, R. Richter, S. Stranges, and F. Vecchiocattivi, *J. Chem. Phys.* **136**, 204302 (2012).
- [30] L. Wei, S. Chen, Y. Zhang, B. Wang, W. Yu, B. Ren, J. Han, Y. Zou, L. Chen, and B. Wei, *Eur. Phys. J. D* **74**, 133 (2020).
- [31] H. Yuan, Sh. Xu, T. Li, Y. Liu, D. Qian, D. Guo, X. Zhu, and X. Ma, *Phys. Rev. A* **102**, 062808 (2020).
- [32] L. Chen, X. Shan, E. Wang, X. Ren, X. Zhao, W. Huang, and X. Chen, *Phys. Rev. A* **100**, 062707 (2019).
- [33] Y. Zhang, X. Wang, D. Lu, B. Wei, B. H. Zhang, Y. J. Tang, R. Hutton, and Y. Zou, *Nucl. Instrum. Methods Phys. Res. B* **337**, 39 (2014).
- [34] I. Bocharova, R. Karimi, E. F. Penka, J.-P. Brichta, P. Lassonde, X. Fu, J.-C. Kieffer, A. D. Bandrauk, I. Litvinyuk, J. Sanderson, and F. Légaré, *Phys. Rev. Lett.* **107**, 063201 (2011).
- [35] R. Itakura, T. Teramoto, A. Hishikawa, and K. Yamanouchi, in *Ultrafast Optics V*, Springer Series in Optical Sciences, Vol. 132, edited by S. Watanabe (Springer, New York, 2007), p. 375.